mathematics

IMPACT FACTOR 2.2

CITESCORE 4.6

Article

Seawater Continuous-Variable Quantum Key Distribution with Orbital Angular Momentum Multiplexing

Lei Mao, Zhangtao Liang, Weihan Zhang, Hang Zhang and Yijun Wang

Topic

Quantum Information and Quantum Computing, 2nd Volume

Edited by

Dr. Durdu Guney and Dr. David Petrosyan

MDPI

https://doi.org/10.3390/math14040660

mathematics

MDPI

Article

Seawater Continuous-Variable Quantum Key Distribution with Orbital Angular Momentum Multiplexing

Lei Mao [1], Zhangtao Liang [1], Weihan Zhang [2], Hang Zhang [1,*] and Yijun Wang [1,*]

[1] School of Automation, Central South University, Changsha 410083, China
[2] School of Computer Science, Beijing University of Posts and Telecommunications, Beijing 100876, China
* Correspondence: zhang22@csu.edu.cn (H.Z.); xxywyj@sina.com (Y.W.)

Abstract

Continuous-Variable Quantum Key Distribution (CVQKD), based on quantum mechanical principles, offers theoretically unconditional security and represents a crucial direction for future secure communications. However, its application in marine environments faces challenges such as high attenuation, scattering, and turbulence in seawater, severely impacting quantum signal transmission and secure key generation efficiency. Orbital angular momentum (OAM) multiplexing technology leverages the orthogonality of photon OAM modes to transmit multiple independent quantum signals in parallel within a single spatial channel. In this scheme, each OAM mode serves as an independent sub-channel, enabling simultaneous key distribution across multiple modes, thereby significantly enhancing the system's secure key rate and spectral efficiency. This paper proposes an OAM-multiplexed CVQKD scheme tailored for marine channels. Based on Yi's power spectrum model for marine turbulence refractive index fluctuations, we derive expressions for OAM mode probability density and detection probability. Through system modeling and performance analysis, we investigate the impact of marine turbulence on OAM modes, as well as on the secure key rate and transmission distance of CVQKD systems. Results indicate that higher-order OAM modes exhibit more pronounced turbulence effects, leading to reduced key rates and limited transmission distances. The OAM multiplexing approach significantly enhances system key rates, providing theoretical and technical references for constructing high-rate seawater quantum communication networks.

Keywords: Continuous-Variable Quantum Key Distribution; orbital angular momentum; oceanic turbulence; seawater quantum communication; secret key rate

MSC: 81P45

Academic Editor: João Nuno Prata

Received: 23 January 2026
Revised: 8 February 2026
Accepted: 11 February 2026
Published: 13 February 2026

1. Introduction

As the pace of global digitalization accelerates, the security of information transmission has risen to unprecedented strategic importance. Quantum key distribution (QKD) technology [1,2], as an encryption method based on fundamental principles of quantum mechanics, theoretically offers information-theoretically provable unconditional security and has emerged as a core candidate for next-generation secure communications. Compared to discrete-variable quantum key distribution (DVQKD) relying on single-photon detection, CVQKD [3,4] offers multiple practical advantages in underwater environments: it is compatible with classical optical components operating at conventional telecommunication wavelengths, achieves higher detection efficiency under high-loss conditions, and holds the

potential for higher key rates under moderate channel loss conditions. However, extending CVQKD applications from ideal fiber-optic links to complex marine environments [5,6] presents a series of formidable challenges. The inherent strong attenuation, scattering effects, and complex turbulent perturbations [7,8] in seawater channels severely constrain the fidelity transmission of quantum signals and the generation efficiency of secure keys.

To overcome the bottlenecks in channel capacity and key generation rate, orbital angular momentum multiplexing technology [9] is regarded as a highly promising solution. Photonic OAM provides a theoretically infinite-dimensional and mutually orthogonal Hilbert space, enabling the parallel transmission of multiple independent data streams within the same spatial mode and wavelength. This holds the potential for enhancing channel capacity [10,11]. The integration of OAM multiplexing with CVQKD [12,13] constitutes an attractive research frontier aimed at constructing high-speed, highly secure underwater quantum secure communication networks. Nevertheless, deploying OAM-based CVQKD systems in seawater channels faces multiple physical constraints. Primarily, ocean turbulence is the primary factor causing OAM mode degradation. Random refractive index fluctuations caused by uneven distributions of seawater temperature and salinity disrupt the helical wavefront structure of vortex beams, inducing inter-mode crosstalk and energy diffusion, which subsequently reduces the detection probability at the receiver [14]. Second, the absorption and scattering effects of seawater [15] not only cause extremely high channel losses but also introduce complex non-Gaussian noise, posing additional challenges for CVQKD security analysis and parameter estimation.

For underwater OAM quantum communication, Bouchard et al. [16] completed an underwater quantum communication experiment based on photon orbital angular momentum. They compared different quantum cryptographic protocols in underwater quantum channels, demonstrating the feasibility of high-dimensional encoding schemes underwater. Cheng et al. [17] employed the Rytov approximation theory to analyze the impact of oceanic turbulence factors on the spiral spectrum of orbital angular momentum. Results indicate that OAM signal photons in different modes experience crosstalk under oceanic turbulence. Currently, domestic and international studies on the influence of oceanic turbulence on OAM quantum communication performance are based on the Nikishov oceanic turbulence model [18], which simplistically assumes stable stratification of seawater. The Nikishov spectrum deviates from the Obukhov-Corrsin law in the inertial-convective regime and shows significant differences from the Kraichnan spectrum in the viscous-convective regime. To overcome these limitations, Yi [19] proposed a novel ocean refractive index fluctuation spectrum model capable of reflecting OAM beam propagation in more complex ocean turbulence.

This paper proposes a CVQKD with OAM multiplexing scheme for marine channels and analyzes its performance. First, the marine power-law spectrum of refractive index fluctuations proposed by Yi is introduced. Subsequently, expressions for the OAM mode probability density and detection probability are derived using Yi's spectrum under marine turbulence conditions. Second, the transmission process of the CVQKD with OAM multiplexing scheme is described in detail. Finally, the performance of this scheme is analyzed to demonstrate the security of OAM-based CVQKD systems. In such systems, a larger angular mode number results in more pronounced effects of ocean turbulence on the modes, leading to lower key rates and shorter maximum transmission distances. Furthermore, by comparing the performance of multiplexed and non-multiplexed schemes, we find that OAM multiplexing significantly enhances the system key rate.

The remainder of this paper is structured as follows: Section 2 analyzes the impact of ocean turbulence on OAM beams; Section 3 details our proposed CVQKD with OAM mul-

tiplexing scheme; Section 4 evaluates system performance and conducts security analysis of the scheme; finally, Section 5 summarizes the research and presents conclusions.

2. Oceanic Turbulence Effects on OAM

2.1. Oceanic Refractive Index Spectrum Model

When light propagates through turbulent or other randomly inhomogeneous media, its amplitude, phase, and arrival angle undergo random perturbations. Studying this process is crucial for understanding the interaction between light and complex media. The refractive index of seawater primarily depends on temperature and salinity. Within the inertial convection zone, it exhibits turbulence similar to atmospheric turbulence, but becomes more complex at smaller scales: viscosity significantly affects velocity fluctuations, while thermal diffusion and salt diffusion have negligible effects on temperature-salinity fluctuations. Therefore, it is necessary to establish a functional relationship between refractive index perturbations and temperature-salinity gradients. This study employs the ocean refractive index fluctuation spectrum model proposed by Yi to analyze the power spectrum function of ocean turbulence.

An oceanic scalar fluctuation spectrum should satisfy two conditions: first, it should possess a mathematical form convenient for analysis; second, it should conform to the Obukhov-Corrsin law in the inertial subrange and align with the Kraichnan spectrum (with constant $q_k = 5.26$) in the viscous subrange. The scalar spectrum can be expressed as [20]:

$$E_s(\kappa) = \beta\chi\epsilon^{-1/3}\kappa^{-5/3}g(\kappa\eta, \mathrm{Pr}), \tag{1}$$

where κ is the spatial wavenumber, β is the Obukhov–Corrsin constant, χ represents the scalar dissipation rate, ϵ is the turbulent kinetic energy dissipation rate, η is the Kolmogorov microscale, Pr and is the Prandtl number. Here, $g(\kappa\eta, \mathrm{Pr})$ is a dimensionless function that approaches 1 when $\kappa\eta \ll 1$ and approaches 0 when $\kappa\eta \gg 1$. This function shows an increasing trend in the viscous-convective range $(1/\eta \ll \kappa \ll 1/\eta_\beta)$ and exhibits exponential decay in the viscous-diffusive range $(\kappa \gg 1/\eta_\beta)$. Employing a method similar to Frehlich [21], we take:

$$g(\kappa\eta, \mathrm{Pr}) = \left[1 + \sum_{n=1}^{M} a_n(\kappa\eta)^*\right] \exp(-\delta\kappa\eta), \tag{2}$$

For water temperature conditions $(\mathrm{Pr} = 7)$, we set $M = 5$, with coefficients:

$$a_1 = 5.1615,\ a_2 = 67.1941,\ a_3 = -45.918\ a_4 \quad = 53.3589,\ a_5 = 1.2064,\ \delta = 3.3927, \tag{3}$$

This yields the normalized dissipation form of the scalar fluctuation spectrum:

$$\frac{(\kappa\eta_B)^2 E(\kappa)}{\chi(\nu/\epsilon)^{1/2}\eta_B} = \beta \mathrm{Pr}^{-1/3}(\kappa\eta_B)^{1/3}\left[1 + \sum_{n=1}^{N} a_n\left(\mathrm{Pr}^{1/2}(\kappa\eta_B)^*\right)\right] \exp\left(-\delta \mathrm{Pr}^{1/2}\kappa\eta_B\right), \tag{4}$$

where χ_T, χ_S, and χ_{TS} represent the dissipation rates of mean square temperature fluctuations, mean square salinity fluctuations, and the covariance between temperature and salinity, respectively. The refractive index fluctuation power spectrum is represented by the combined contributions of the temperature spectrum, salinity spectrum, and their cospectrum:

$$E_\kappa(\kappa) = A^2 E_T(\kappa) + B^2 E_S(\kappa) - 2AB E_{TS}(\kappa), \tag{5}$$

where A is the thermal expansion coefficient and B is the saline contraction coefficient. Here, E_T and E_S denote the power spectra of temperature and salinity fluctuations, respectively,

while E_{TS} represents their cospectrum. The negative sign in the cross term accounts for the anticorrelation between temperature and salinity fluctuations in typical oceanic conditions.

Substituting the scalar spectral form gives:

$$E_\kappa(\kappa) = A^2\beta\chi_T\epsilon^{-1/3}\kappa^{-5/3}\left[g(\kappa\eta, \mathrm{Pr}T) + \frac{dr}{\omega^2}g(\kappa\eta, \mathrm{Pr}S) - \frac{1+dr}{\omega}g(\kappa\eta, \mathrm{Pr}TS)\right], \quad (6)$$

The corresponding three-dimensional spatial power spectrum is:

$$\Phi n(\kappa) = (4\pi)^{-1}A^2\beta\chi_T\epsilon^{-1/3}\kappa^{-11/3}\left[g(\kappa\eta, \mathrm{Pr}T) + \frac{dr}{\omega^2}g(\kappa\eta, \mathrm{Pr}S) - \frac{1+dr}{\omega}g(\kappa\eta, \mathrm{Pr}_{TS})\right], \quad (7)$$

2.2. Detection Probability of OAM

In turbulent channels, refractive index fluctuations caused by random variations in the turbulent medium lead to random phase fluctuations of the beam, scattering the input state in a finite-dimensional OAM space onto neighboring OAM modes, thereby affecting detection probability. The following derivation models the propagation of a partially coherent Laguerre–Gaussian beam through oceanic turbulence. We start from the Rytov perturbation theory under weak fluctuation conditions, and derive the cross-spectral density function to quantify the OAM mode crosstalk and detection probability. According to the Rytov perturbation theory, when an optical wave propagates under weak fluctuation conditions (i.e., satisfying $q = z/k\rho_0^2 < 1$ and $q\Lambda < 1$, where k is the optical wavenumber, ρ_0 is the spatial coherence radius of a plane wave, and Λ is the Gaussian beam spot parameter at the receiver), the complex amplitude of a partially coherent Laguerre Gauss (LG) beam in the half-space $z > 0$ can be expressed in cylindrical coordinates (r, ϕ, z) as:

$$LG_{\psi,\rho_0}(r, \phi, z) = LG^{\mathrm{free}}_{\psi,\rho_0}(r, \phi, z)\exp[\psi_1(r, \phi, z)], \quad (8)$$

Here, $LG^{\mathrm{free}}_{l_0,p_0}(r, \phi, z)$ represents the normalized partially coherent LG mode field distribution at the receiver plane z in the absence of turbulence, where l_0 and p_0 correspond to the azimuthal (topological charge) and radial orders, respectively; r is the two-dimensional position vector on the source plane; ϕ is the azimuthal angle; $\psi_1(r, \phi, z)$ characterizes the complex phase random perturbation induced by oceanic turbulence; z is the beam propagation distance. Under the paraxial approximation framework, the complex amplitude of a partially coherent LG beam in a turbulence-free channel can be expressed as:

$$LG^{\mathrm{free}}_{l_0,p_0}(r, \phi, z) = (2\pi)^{-4/2}R_{l_0,p_0}(r, z)\exp(il_0\phi), \quad (9)$$

where $R_{l_0,p_0}(r, z)$ is the radial basis function describing the transverse beam distribution, with the specific form [22]:

$$\begin{aligned} R_{l_0,p_0}(r, z) = {} & \frac{1}{\omega_z}\sqrt{\frac{2p_0!}{\pi(p_0 + |l_0|)!}}\left(\frac{r\sqrt{2}}{\omega_z}\right)^{l_0} L^{l_0}_{p_0}\left(\frac{2r^2}{\omega_z^2}\right) \\ & \times \exp\left\{-\frac{r^2}{\omega_z^2} - \frac{ikr^2z}{2(z^2 + z_R^2)} + i(2p_0 + |l_0| + 1)\theta\right\}, \end{aligned} \quad (10)$$

Here, $\omega_z = \omega_0\sqrt{1 + (z/z_k)^2}$ denotes the beam spot size after propagating distance z, ω_0 is the initial beam width at the transmitter, $z_k = k\omega_0^2/2$ is the Rayleigh length, $k = 2\pi/\lambda$ is the wavenumber, λ is the optical wavelength, $L^{l_0}_{p_0}(\cdot)$ is the generalized Laguerre polynomial, and $\theta = \tan^{-1}(z/z_k)$ is the Gouy phase.

For a paraxial beam, the second-order cross-spectral density function of a partially coherent LG beam after propagation through an oceanic turbulent channel can be written as [23]:

$$W(\mathbf{r},\mathbf{r}',z) = \left\langle LG_{l_0,p_0}(\mathbf{r},z)LG^{*}_{l_0,p_0}(\mathbf{r}',z)\right\rangle, \tag{11}$$

Here, $\langle\cdot\rangle$ denotes the ensemble average over both the random fluctuations of the partially coherent source and the random phase perturbations induced by oceanic turbulence, and the superscript $*$ denotes the complex conjugate. Assuming statistical independence between the source fluctuations and oceanic turbulence, the cross-spectral density function can be decomposed as:

$$W(\mathbf{r},\mathbf{r}',z) = \alpha(\mathbf{r},\mathbf{r}')\left\langle LG^{\text{free}}_{l_0,p_0}(\mathbf{r},z)LG^{\text{free}*}_{l_0,p_0}(\mathbf{r}',z)\right\rangle_T, \tag{12}$$

where $\alpha(\mathbf{r},\mathbf{r}')$ is the normalized coherence function, and the subscript T indicates averaging solely over turbulent fluctuations.

Under free-space propagation conditions, the normalized coherence function of a partially coherent LG beam remains unchanged with propagation distance, identical to that at the source plane $z = 0$. Adopting a Gaussian coherence function model [24]:

$$\alpha(\mathbf{r},\mathbf{r}') = \exp\left(-\frac{|\mathbf{r}-\mathbf{r}'|^2}{\rho_z^2}\right), \tag{13}$$

where ρ_s is the spatial coherence length at the source plane.

Using the quadratic approximation for the wave structure function:

$$\left\langle \exp\left[\psi_1(\mathbf{r},z)+\psi_1^{*}(\mathbf{r}',z)\right]\right\rangle_T \approx \exp\left(-\frac{|\mathbf{r}-\mathbf{r}'|^2}{\rho_0^2}\right), \tag{14}$$

Here, ρ_0 denotes the spatial coherence radius of a spherical wave in oceanic turbulence, expressed as:

$$\rho_0 = \left[\frac{\pi^2k^2z}{3}\int_0^{\infty}\kappa^3\Phi_n(\kappa),d\kappa\right]^{-1/2}, \tag{15}$$

where $\Phi_n(\kappa)$ is the oceanic turbulent refractive index fluctuation power spectrum established in Section 2.1 based on Yi's model, and κ is the spatial frequency. After derivation, ρ_0 can be further simplified to:

$$\rho_0 = \left[8.44\pi k^2z,\beta\chi_r e^{-1/3}\eta^{-1/3}\right]^{-1/2}, \tag{16}$$

Research shows that oceanic turbulence can alter the OAM mode composition of partially coherent LG beams, whereas these modes can remain stable in free space. Consequently, the perturbed optical field can be expanded as a linear superposition of a set of eigenmodes:

$$LG_{l_v,\rho_0}(\mathbf{r},z) = (2\pi)^{-1/2}\sum_{l_v,p}\Omega_{l_v,p}(z)LG^{\text{fres}}_{l_v,p}(\mathbf{r},z), \tag{17}$$

The expansion coefficients $\Omega_{l_v,p}(z)$ are given by:

$$\Omega_{l_v,p}(z) = (2\pi)^{-1/2}\int_0^{2\pi}R_{l_v,p}(r,z)\exp(-il\phi)LG_{l_v\rho_s}(\mathbf{r},z),d\phi, \tag{18}$$

After performing the statistical average over turbulent fluctuations, the mode probability density corresponding to eigenstate (l,p) is obtained:

$$\left\langle \left|\Omega_{l,p}(z)\right|^2 \right\rangle = \frac{1}{4\pi^2}\iint d\phi d\phi', R_{l,p}(r,z)R_{l,p}^{(r',z)}R_{l_0,p_0}(r,z)R_{l_0,p_0}^{(r',z)} \times \exp\left[i(l_0-l)(\phi-\phi') - \frac{|\mathbf{r}-\mathbf{r}'|^2}{\rho_0^2}\right], \tag{19}$$

Introducing the effective spatial coherence length $\tilde{\rho}0 = a_0\rho_0$, where $a_0 = (1+\rho_0^2/\rho_s^2)^{-1/2}$, and utilizing the completeness relation of the radial basis functions, the expression for the OAM mode probability density of a partially coherent LG beam after transmission through oceanic turbulence is obtained:

$$\left\langle |\Omega_l(z)|^2 \right\rangle = \frac{p_0!}{\pi^2\omega_z^2(p_0+|l_0|)!}\left(\frac{2r^2}{\omega_z^2}\right)^{|l_0|}\left|L_{p_0}^{l_0}!\left(\frac{2r^2}{\omega_z^2}\right)\right|^2 \exp\left(-\frac{2r^2}{\omega_z^2}-\frac{2r^2}{\tilde{\rho}0^2}\right) I|l-l_0|!\left(\frac{2r^2}{\tilde{\rho}_0^2}\right), \tag{20}$$

Here, $In(\cdot)$ denotes the modified Bessel function of the first kind of order n. Finally, the weight (i.e., mode probability) of each OAM mode l on the receiver plane can be obtained via:

$$P_l = \frac{\int_0^\infty \langle |\Omega_l|^2 \rangle r, dr}{\sum_l \int_0^\infty \langle |\Omega_l|^2 \rangle r, dr'}, \tag{21}$$

Based on theoretical derivations, this study calculates and demonstrates the OAM mode probability density and detection probability of partially coherent LG beams in oceanic turbulence. The turbulence spectrum model employed is based on that proposed by Yi [25]. Figure 1a shows that the peak of the probability density $\langle |\Omega_l(z)|^2 \rangle$ gradually decreases as the azimuthal mode order l increases, and the position of the peak also moves further away from the beam center $(r = 0)$ with increasing order. This indicates that selecting an appropriate angular mode order is crucial for enhancing OAM detection efficiency during CVQKD in oceanic turbulence. Figure 1b further demonstrates that the detection probability decreases overall with increasing angular mode order l. This is attributed to the larger effective radius of higher-order beams, which experience more pronounced turbulence-induced wavefront perturbations. Consequently, phase distortion and beam spreading effects intensify, adversely affecting system detection performance.

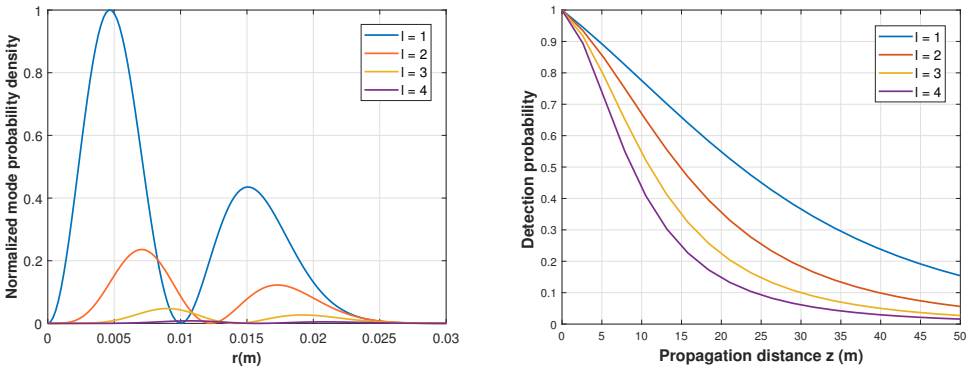

(**a**) (**b**)

Figure 1. The mode probability density and detection probability of the LG beam under different values of l (**a**) Mode probability density of LG beams in oceanic turbulence against r for different values of l. (**b**) Detection probability for LG beams in oceanic turbulence against z for different values of l.

Figure 2a shows that under different turbulent kinetic energy dissipation rates ϵ, the detection probability decreases as ϵ diminishes. The smaller the ϵ, the slower the turbulent energy transfer becomes; however, the phase perturbations experienced by the beam become more persistent and complex, leading to increased wavefront distortion and expan-

sion, which degrades detection capability. Figure 2b indicates that the detection probability drops sharply as the mean square temperature dissipation rate χ_T increases. An increase in χ_T reflects intensified temperature fluctuation dissipation and enhanced turbulent thermal mixing, leading to amplified refractive index fluctuations. This exacerbates beam scattering and phase interference, making OAM modes more susceptible to decoherence and crosstalk, thereby causing a rapid decrease in detection probability.

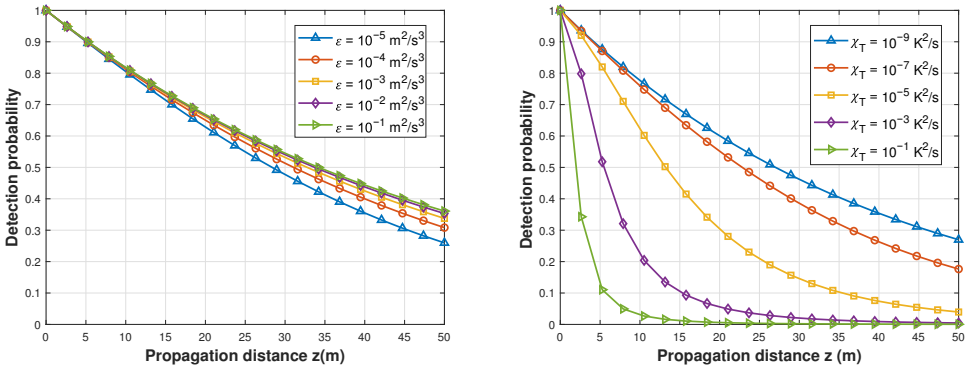

(**a**) (**b**)

Figure 2. Detection probability for LG beams in oceanic turbulence against z for ϵ and χ_T. (**a**) Detection probability of different ϵ. (**b**) Detection probability of different χ_T.

3. Seawater CVQKD with OAM Multiplexing

This section proposes and elaborates on a CVQKD system scheme based on OAM multiplexing, detailing its overall architecture and key operational procedures. Leveraging the spatial orthogonality of OAM modes, this approach enables parallel transmission of multiple quantum signals within the same optical channel, thereby enhancing both the key generation rate and spectral efficiency of the CVQKD system. As shown in Figure 3, the system schematic encompasses the complete process from signal preparation, modulation, multiplexing, and channel transmission to demodulation, detection, and post-processing. The specific steps are as follows:

- Step 1: The transmitter (Alice) generates a continuous-wave laser beam, which is split into two paths by a polarization beam splitter (PBS): one path carries the signal light with lower intensity for quantum information transmission; the other path carries the local oscillator (LO) light with higher intensity, providing a phase reference for subsequent coherent detection.
- Step 2: The signal light first enters a set of beam splitters (BS), where it is uniformly divided into four independent branches. Each signal branch undergoes combined modulation through an amplitude modulator (AM) and a phase modulator (PM) to encode and generate four distinct quantum states. The modulated sub-beams are then attenuated to single-photon-level low power levels before being incident onto different spatial light modulators (SLM_A^i). Each SLM_A^i is loaded with a phase hologram possessing a specific topological charge value, thereby transforming the corresponding Gaussian beam into LG beams carrying distinct OAM modes. These signal beams, each bearing a different OAM state, are subsequently fed into an OAM multiplexing module for beam combining. The combined beam then passes through a polarization beam splitter (PBS) to couple with the local oscillator light, forming the composite output beam.

- Step 3: The composite beam is transmitted through the ocean channel to the receiver (Bob). This channel model accounts for practical attenuation and noise factors such as transmittance T_{sea} and excess noise ε_{noise}. Upon receiving the signal, Bob first uses a PBS to separate the composite beam back into the signal beam and the local oscillator beam. The signal beam enters the OAM demultiplexing module, where it is separated into four corresponding channels based on mode orthogonality. Each channel's beam then undergoes demodulation via an SLM_B^i. The phase pattern loaded onto this SLM_B^i matches the complex conjugate of the corresponding pattern at Alice's end, completing the inverse conversion of the OAM mode. Simultaneously, the local oscillator beam is uniformly divided into four paths via another beam splitter network. These four paths interfere with the four demodulated signal beams in a balanced homodyne detector, enabling measurement of each signal. The detection process accounts for non-ideal factors such as the detector's efficiency η and electron noise velocity v_{el}.
- Step 4: Bob transmits the measurement results to Alice via the classical channel. Both parties sequentially perform post-processing operations—including parameter estimation, reverse reconciliation and privacy amplification on the acquired data, ultimately extracting a secure key.

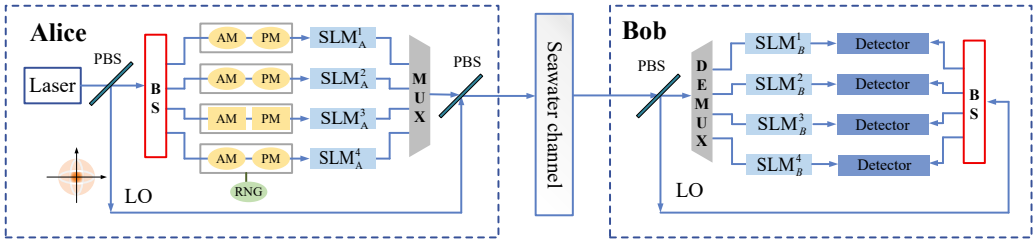

Figure 3. The system layout of seawater CVQKD with OAM Multiplexing. AM, amplitude modulator; PM, phase modulator; RNG, random number generator; MUX, multiplexing; DEMUX, demultiplexing; SLM, spatial light modulator; PBS, polarization beam splitter; BS, beam splitters.

4. Performance Analysis

To evaluate the security and performance of the proposed OAM-multiplexed CVQKD system, we consider collective attacks in the asymptotic regime. The secret key rate is derived based on the Shannon mutual information between Alice and Bob and the Holevo bound between Bob and Eve. The channel transmittance incorporates both seawater attenuation and OAM mode detection probability derived in Section 2.2. As discussed in Section 2.2, different OAM modes exhibit varying detection probabilities, which will influence the final key rate. The probability distribution of transmittance in the seawater channel can be described by Beer's law. When neglecting the multiple scattering of photons during point-to-point signal propagation, the deterministic loss caused by oceanic extinction affects the transmission probability. Combining this with the detection probability formula in Section 2.2, the transmittance can be expressed as [26]:

$$T_{\text{sea}} = \exp[-(a(\lambda, d) + b(\lambda, d))z] \cdot P_l, \tag{22}$$

where $a(\lambda, d)$ and $b(\lambda, d)$ denote the absorption coefficient and the scattering coefficient of light with wavelength λ, depth d and transmission distance z, P_l denotes the detection probability for Section 2.2.

Crosstalk noise between different OAM modes caused by atmospheric turbulence, which can be expressed as

$$\varepsilon_{\text{noise}} = \varepsilon_0 + \frac{\tau P_{\text{crosstalk}}}{h v_c}, \tag{23}$$

where $\tau = 1$ ns is the effective sampling period of the heterodyne detector, h is the Planck constant, and v_c is the frequency of the noise photon satisfying $hv_c = 1.28 \times 10^{-19}$ J. $P_{\text{crosstalk}}$ is the noise power induced by crosstalk with

$$P_{\text{crosstalk}} = \sum_{i=1}^{n} P_l \cdot P_{\text{in}}, \tag{24}$$

where P_l denotes the detection probability for Section 2.2. Additionally, P_{in} is the input power of the OAM beam.

Through theoretical derivation, we have obtained the asymptotic secret key rate for collective attacks:

$$K = \sum_{i=1}^{n} [I_{AB}(l_i) - \chi_{BE}(l_i)], \tag{25}$$

where C_M represents the capacity of the main channel, C_W is the capacity of the wiretapping channel, i is the number of multiplexes. I_{AB} represents the Shannon mutual information between Alice and Bob, χ_{BE} represents the Holevo bound between Bob and Eve in the protocol. For heterodyne detection, I_{AB} can be expressed as

$$I_{AB} = \frac{1}{2}\log_2\left(\frac{V + \chi_{\text{tot}}}{1 + \chi_{\text{tot}}}\right), \tag{26}$$

where $V = V_A + 1$, V_A is the modulation variance, the total noise $\chi_{\text{tot}} = \chi_{\text{line}} + \chi_{\text{hom}} / T_{\text{sea}}$, the channel linear noise $\chi_{\text{ime}} = 1/T_{\text{sea}} + \varepsilon_{\text{noise}} - 1$, and the homodyne detection noise $\chi_{\text{hom}} = (2 + 2v_{el} - \eta_{det})/\eta_{det}$. χ_{BE} can be calculated, namely

$$\chi_{BE} = \sum_{i=1}^{2} G\left(\frac{\lambda_i - 1}{2}\right) - \sum_{i=3}^{5} G\left(\frac{\lambda_i - 1}{2}\right), \tag{27}$$

where $G(x) = (x+1)\log_2(x+1) - x\log_2(x)$.The symplectic eigenvalues $\lambda_{1,2}$ are as follows:

$$\lambda_{1,2} = \sqrt{\frac{1}{2}\left(A \pm \sqrt{A^2 - 4B}\right)}, \tag{28}$$

where

$$A = V^2 + T_{sea}^2(V + \chi_{\text{line}})^2 - 2T_{sea}(1 - V)^2, B = T_{sea}^2(1 + V\chi_{\text{line}})^2. \tag{29}$$

The symplectic eigenvalues $\lambda_{3,4,5}$ are as follows:

$$\lambda_{3,4} = \sqrt{\frac{1}{2}\left(C \pm \sqrt{C^2 - 4D}\right)}, \lambda_5 = 1, \tag{30}$$

where

$$C = \frac{A\chi_{\text{hom}} + V\sqrt{B} + T_{sea}(V + \chi_{line})}{T_{sea}(V + \chi_{tot})}, D = \frac{\sqrt{B}V + B\chi_{\text{hom}}}{T_{sea}(V + \chi_{tot})}. \tag{31}$$

Through the aforementioned analysis, the impact of OAM angular modulus on CVQKD system performance can be evaluated. As depicted in Figure 4a, the relationship curves between lower-layer system security capacity and transmission distance are presented for different scenarios. Simulation results indicate that both the system security key rate K and transmission distance z gradually decrease as the angular modulus l increases. As depicted in Figure 4b, we simulated the relationship between key rate and transmission distance in the OAM multiplexed CVQKD protocol, comparing it with the single-mode scenario within the multiplexing scheme. Simulation results indicate that the system's key rate diminishes with increasing transmission distance. Within the multiplexing scheme, the key rate progressively increases with rising multiplexing channels N,

consistently outperforming the single-mode scenario. Consequently, CVQKD with OAM multiplexing enhances the system's key rate, thereby enabling the transmission of greater volumes of secure information.

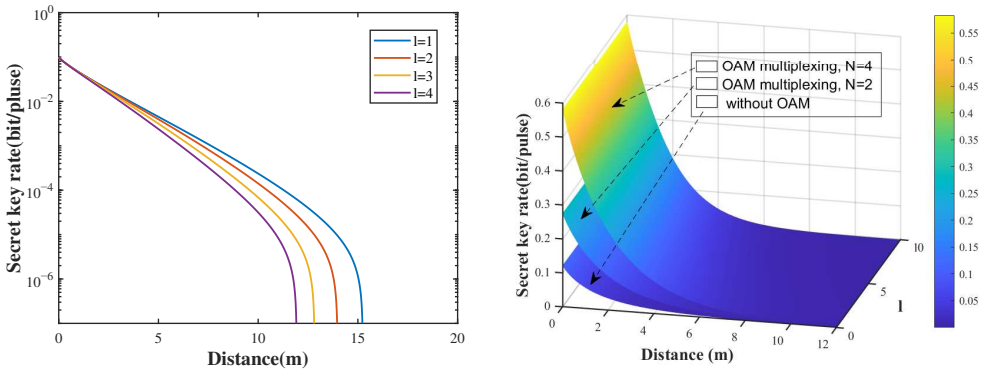

(**a**) (**b**)

Figure 4. Relationship diagram between secret key rate and propagation distance. (**a**) Functional relationship between secret key rate and propagation distance under different angular momentum orbital modes. (**b**) Functional relationship between the secret key rate and the propagation distance of the system with or without OAM multiplexing.

5. Conclusions

This paper addresses the challenges of enhancing channel capacity and key rate for continuous-variable quantum key distribution (CVQKD) systems in marine environments. It proposes a CVQKD scheme based on orbital angular momentum multiplexing and systematically analyzes its performance and security in marine turbulent channels. First, based on the marine turbulent refractive index fluctuation spectrum model proposed by Yi, this paper derives expressions for the probability density of OAM modes and detection probability of partially coherent Laguerre–Gaussian beams propagating through turbulence. It reveals that higher-order OAM modes are more susceptible to turbulence effects, and detection probability decreases with increasing angular mode number. Second, by constructing a model of the OAM multiplexed CVQKD system and incorporating seawater absorption and scattering effects, theoretical expressions for transmission efficiency and key rate were established. Performance analysis indicates that oceanic turbulence parameters (such as the turbulent kinetic energy dissipation rate and temperature dissipation rate) significantly impact the system detection probability. The OAM multiplexing scheme effectively enhances the system key rate, with particularly pronounced performance advantages under multiplexed conditions. Compared to single-mode transmission, the multiplexing scheme achieves higher secure information transmission capacity at equivalent transmission distances.

Although the OAM multiplexed CVQKD scheme proposed in this paper demonstrates theoretical potential for enhancing key rates and transmission capacity, mode crosstalk and wavefront distortion caused by ocean turbulence remain major challenges for practical deployment. To improve system robustness in dynamic marine environments, future research may explore hybrid compensation strategies combining adaptive optics with digital signal processing. Adaptive optics systems can effectively suppress turbulence-induced OAM mode spreading by real-time detection and correction of wavefront aberrations, thereby improving mode purity and detection probability at the receiver. Meanwhile, digital signal processing algorithms based on MIMO technology can equalize and decouple mode crosstalk during post-processing, further mitigating cross-channel interference. Integrating adaptive optics' front-end correction with digital signal processing's back-end equalization

holds promise for achieving stable, efficient quantum key distribution in highly turbulent, high-loss marine channels. Furthermore, deep learning-based channel prediction and compensation methods warrant deeper exploration in future work to advance underwater quantum communication from theory to engineering practice.

Author Contributions: Conceptualization, L.M. and Y.W.; methodology, L.M. and H.Z.; software, L.M. and Z.L.; validation, L.M. and W.Z.; formal analysis, L.M. and W.Z.; investigation, L.M.; data curation, L.M. and Z.L.; writing—original draft preparation, L.M.; writing—review and editing, H.Z. and Y.W. All authors have read and agreed to the published version of the manuscript.

Funding: This work was funded by the Ye Qixun Science Fund of the National Natural Science Foundation of China (Grant No. U2441219).

Institutional Review Board Statement: The study did not require ethical approval.

Data Availability Statement: The original contributions presented in this study are included in the article. Further inquiries can be directed to the corresponding authors.

Conflicts of Interest: The authors declare no conflicts of interest.

References

1. Li, Y.; Cai, W.-Q.; Ren, J.-G.; Wang, C.-Z.; Yang, M.; Zhang, L.; Wu, H.-Y.; Chang, L.; Wu, J.-C.; Jin, B.; et al. Microsatellite-based real-time quantum key distribution. *Nature* **2025**, *640*, 47–54. [CrossRef]
2. Zahidy, M.; Mikkelsen, M.T.; Müller, R.; Da Lio, B.; Krehbiel, M.; Wang, Y.; Bart, N.; Wieck, A.D.; Ludwig, A.; Galili, M.; et al. Quantum key distribution using deterministic single-photon sources over a field-installed fibre link. *npj Quantum Inf.* **2024**, *10*, 2. [CrossRef]
3. Zhang, Y.; Bian, Y.; Li, Z.; Yu, S.; Guo, H. Continuous-variable quantum key distribution system: Past, present, and future. *Appl. Phys. Rev.* **2024**, *11*, 011318. [CrossRef]
4. Zheng, X.; Zhang, Q.; Ling, J.; Guo, G.; Han, Z. Free-space continuous-variable quantum key distribution under high background noise. *npj Quantum Inf.* **2025**, *11*, 52. [CrossRef]
5. Wu, X.; Huang, D. Underwater continuous-variable quantum key distribution with faster-than-nyquist scheme. *Quantum Inf. Process.* **2025**, *2*, 24. [CrossRef]
6. Zhu, Y.; Mao, L.; Hu, H.; Wang, Y. Passive Continuous Variable Quantum Key Distribution through the Oceanic Turbulence. *Entropy* **2023**, *25*, 307. [CrossRef]
7. Farwell, N.; Korotkova, O. Intensity and coherence properties of light in oceanic turbulence. *Opt. Commun.* **2012**, *285*, 872–875. [CrossRef]
8. Wu, Y.; Zhang, Y.; Li, Y.; Hu, Z. Beam wander of gaussian-schell model beams propagating through oceanic turbulence. *Opt. Commun.* **2016**, *371*, 59–66. [CrossRef]
9. Allen, L.; Beijersbergen, M.W.; Spreeuw, R.J.C.; Woerdman, J.P. Orbital angular momentum of light and transformation of laguerre gaussian laser modes. *Phys. Rev. A* **1992**, *45*, 8185–8189. [CrossRef]
10. Wang, J.; Yang, J.Y.; Fazal, I.M.; Ahmed, N.; Yan, Y.; Huang, H. Terabit free-space data transmission employing orbital angular momentum multiplexing. *Nat. Photonics* **2012**, *6*, 488–496. [CrossRef]
11. Ren, Y.; Wang, Z.; Liao, P.; Li, L.; Xie, G.; Huang, H. Experimental characterization of a 400 Gbit/s orbital angular momentum multiplexed free-space optical link over 120 m. *Opt. Lett.* **2016**, *41*, 622. [CrossRef] [PubMed]
12. Zhang, H.; Guo, Y.; Shi, W.; Chen, G.; Zhao, W.; Ruan, X. High-rate continuous-variable quantum key distribution with orbital angular momentum multiplexing. *Entropy* **2021**, *23*, 1187.
13. Jin, D.; Guo, Y.; Wang, Y.; Huang, D. Parameter estimation of orbital angular momentum based continuous-variable quantum key distribution. *J. Appl. Phys.* **2020**, *127*, 213102. [CrossRef]
14. Ying, X.; Hai, S.; Yi, Z. Effects of anisotropic oceanic turbulence on the power of the bandwidth-limited OAM mode of partially coherent modified Bessel correlated vortex beams. *J. Opt. Soc. Am. A* **2018**, *35*, 1839–1845. [CrossRef]
15. Gabriel, C.; Khalighi, M.A.; Bourennane, S.; Leon, P.; Rigaud, V. Monte-carlo-based channel characterization for underwater optical communication systems. *J. Opt. Commun. Netw.* **2013**, *5*, 1–12. [CrossRef]
16. Bouchard, F.; Sit, A.; Hufnagel, F.; Abbas, A.; Karimi, E. Quantum cryptography with twisted photons through an outdoor underwater channel. *Opt. Express* **2018**, *26*, 22563. [CrossRef]
17. Cheng, M.; Guo, L.; Li, J.; Huang, Q.; Cheng, Q.; Zhang, D. Propagation of an optical vortex carried by a partially coherent laguerre–gaussian beam in turbulent ocean. *Appl. Opt.* **2016**, *55*, 4642. [CrossRef] [PubMed]

18. Nikishov, V.V.; Nikishov, V.I. Spectrum of turbulent fluctuations of the sea-water refraction index. *Int. J. Fluid Mech. Res.* **2000**, *27*, 82–98. [CrossRef]
19. Xiang, Y.; Djordjevic, I.B. Power spectrum of refractive-index fluctuations in turbulent ocean and its effect on optical scintillation. *Ptics Express* **2018**, *26*, 10188.
20. Muschinski, A.; de Bruyn Kops, S.M. Investigation of hill's optical turbulence model by means of direct numerical simulation. *J. Opt. Soc. Am. A* **2015**, *32*, 2423. [CrossRef] [PubMed]
21. Frehlich, R. Laser scintillation measurements of the temperature spectrum in the atmospheric surface layer. *J. Atmos. Sci.* **1992**, *49*, 1494–1509. [CrossRef]
22. Jiang, Y.S.; Wang, S.H.; Zhang, J.H.; Ou, J.; Tang, H. Spiral spectrum of laguerre–gaussian beam propagation in non-kolmogorov turbulence. *Opt. Commun.* **2013**, *303*, 38–41. [CrossRef]
23. Mandel, L.; Wolf, E. *Optical Coherence and Quantum Optics*; Cambridge University Press: Cambridge, UK, 1995; pp. 68–70.
24. Morris, J.E.; Mazilu, M.; Baumgartl, J.; Cimár, T; Dholakia, K. Propagation characteristics of airy beams: Dependence upon spatial coherence and wavelength. *Opt. Express* **2009**, *17*, 13236. [CrossRef] [PubMed]
25. Yi, X.; Zheng, R.; Yue, P.; Ding, W.; Shen, C. Propagation properties of OAM modes carried by partially coherent LG beams in turbulent ocean based on an oceanic power-law spectrum. *Opt. Commun.* **2019**, *443*, 238–244. [CrossRef]
26. Wu, H.; Liu, X.; Zhang, H.; Ruan, X.; Guo, Y. Performance Analysis of Continuous Variable Quantum Teleportation with Noiseless Linear Amplifier in Seawater Channel. *Symmetry* **2022**, *14*, 997. [CrossRef]